Numerical Study on the Uplift Response of RC Slabs Subjected to Blasts

Sami A. Kilic, A.M.ASCE[1]

Abstract: This study investigated the response of reinforced concrete (RC) slabs in building structures to internal explosions. The performances of two slabs designed in accordance with the protective structural design and conventional gravity design approaches were evaluated in terms of midspan displacements, support rotations, and damage patterns. Data from available slab blast experiments in the open literature were used to validate the methodology. A numerical study was carried out for various high-explosive charges detonated underneath the RC slabs. Detonations were simulated using airblast-loading functions. The flexible boundary conditions for the slabs were provided by a one-story single-bay RC frame consisting of beams and columns. All of the reinforcements of the slabs, beams, and columns were modeled explicitly using line elements inserted into the volumetric finite-element mesh of the concrete material. Envelope values of the rebar rupture strain were also used in the parametric study. Results from the numerical study showed that rebar rupture strain was a key factor in the blast performances of both slabs. Current protective design approaches to RC slabs mainly consider support rotations. It is recommended that rebar rupture strain also be accounted for in protective design. **DOI: 10.1061/(ASCE)CF.1943-5509.0000971.**

Author keywords: Uplift deformation; Reinforced concrete (RC) slab; Gravity design; Protective design; Airblast loading; Finite-element analysis.

Introduction

Bomb attacks on building structures have revealed the vulnerability of conventional floor slabs that are designed to resist gravity loads. The 1993 attack on the World Trade Center caused severe damage to concrete floor slabs on the parking garage level (Longinow and Mniszewski 1996). The 1995 Alfred P. Murrah Federal Building street-level bombing attack induced uplift failure of upper floor slabs due to the lack of tension reinforcement (FEMA 1996, 2005). Another case study is the 2003 explosion of a bomb inside the trunk of a car in the parking garage of the El Nogal Club Building in Bogota, Colombia. The forensic investigation of that event presented evidence that the explosion caused more damage to the upper-floor slabs compared with slabs located below the detonation (Garcia et al. 2006). All of these vehicle bombing attacks have emphasized the importance of determining the response of reinforced concrete (RC) slabs in structures subjected to blast loads.

The conventional design approach to RC slabs only considers factored gravity loads for reinforcement sizing and detailing. Continuous reinforcement is provided at the bottom of the slab cross section for the full span. Upper reinforcement is only provided at the support regions because the upper part of the slab cross section is subjected to tensile stresses at the support regions and compressive stresses in the midspan. However, a detonation occurring underneath a floor slab triggers an uplift deformation and may lead to severe damage owing to the lack of tension reinforcement in the midspan. Conventionally designed floor slabs have a limited capacity to mitigate damage caused by uplift blast pressure (FEMA 2008). Slab failure and fragment impacts may subsequently lead to structural damage and threaten lives.

Damage to the floor slabs of building structures can be decreased via protective structural engineering design measures. In contrast to conventional gravity load design, the protective design approach considers uplift blast loads acting on the slab by providing continuous reinforcements at the top and bottom of the cross section throughout the span.

RC slabs ultimately fail in a tensile membrane mode if the main longitudinal reinforcement extends across the entire span of the slab and is properly anchored to the adjacent beams (Krauthammer 2008). Tensile membrane action occurs under excessive deformations of the slab. It is terminated when the reinforcement begins to rupture (Park and Gamble 2000). Therefore, rebar rupture strain plays an important role in the ultimate failure mode of RC slabs going through a tensile membrane action before the start of the disintegration process of the slab, and fragment communication to adjacent structural members.

The protective design approach certainly provides an advantage because the top and bottom longitudinal reinforcements are continuous across the entire span of the slab. However, the gravity design approach also provides blast resistance to the slab if continuous lower longitudinal reinforcements are properly anchored to the adjacent beams. Evaluating the blast resistance of gravity-designed slabs may be of interest to structural design engineers; such information is not available in protective design codes.

Experimental data are crucial to quantifying the response of a slab under a blast loading. A search of the open literature yielded only a single study, conducted by Lawver et al., involving a full-scale experimental investigation of gravity load–designed two-way RC slabs subjected to blast uplift loads (Lawver et al. 2003). However, this study was carried out for a single value of a scaled distance and did not provide explicit information about charge weight and standoff distance.

[1]Assistant Professor, Dept. of Civil Engineering, Bogazici Univ., Bebek, Istanbul 34342, Turkey. E-mail: skilic@boun.edu.tr

Note. This manuscript was submitted on March 14, 2016; approved on September 2, 2016; published online on November 10, 2016. Discussion period open until April 10, 2017; separate discussions must be submitted for individual papers. This paper is part of the ***Journal of Performance of Constructed Facilities***, © ASCE, ISSN 0733-9445.

Because the open literature yielded limited information regarding the uplift blast response of slabs, detonations occurring underneath slabs were investigated in this study.

The commercial finite-element code *LS-Dyna* (LSTC 2015) was used to simulate the blast response of RC slabs. The open literature was searched for blast experiments conducted on two-way RC slabs. The numerical tool was validated by comparing the results of the *LS-Dyna* code against the experimental results of an RC slab obtained from the open literature.

In the second part of this study, a parametric numerical investigation was conducted on two-way RC slabs. Two slabs were designed according to the gravity design procedures in American Concrete Institute (ACI) 318-14 (ACI 2014) and the protective design methodology in Unified Facilities Criteria (UFC) UFC-3-340-02 (DoD 2008). The slabs were considered as surrogates of the floor system in a parking structure. Blast loads were applied to the bottom surfaces of the slabs. The detonation point was chosen as approximately two-thirds of the story height below the bottom surfaces of the slabs, which corresponded to the blast scenario of a bomb exploding in the trunk of a car. A frame consisting of four edge beams and corner columns provided flexible support to the slabs. All of the reinforcement rebars of the beams, columns, and slabs were explicitly modeled with line elements in the parametric study in order to create a high-fidelity numerical model. Various high-explosive charge weights were detonated under the slab at the constant standoff distance of two-thirds the height of the frame. The blast performances of the gravity and protective slab designs with different rebar rupture strains were evaluated.

In the context of a numerical parametric study, this paper presents the following new key contributions: (1) the uplift blast performances of conventional and protective slab designs, quantified according to the support rotations and midspan displacement histories resulting from various charge weight detonations; (2) the numbers of ruptured rebars for the upper and lower longitudinal reinforcements; (3) the failure modes of the slabs along with the crack damage patterns; and (4) the effects of rebar rupture strain on the uplift blast response of the slabs.

Description of the Numerical Approach

The *LS-Dyna* finite-element code with the central difference explicit time marching scheme was employed to investigate transient blast effects on RC slabs (Hallquist 2006). This section describes the nonlinear material models and blast-loading details.

Airblast Loading

The conventional weapons (CONWEP) airblast-loading function of the *LS-Dyna* code was used to simulate the detonation effects of conventional weapons (Hallquist 2006; Randers-Pehrson and Bannister 1997). CONWEP originates from the computer code developed by Hyde (1993), who implemented available empirical polynomial functions obtained by applying curve-fitting techniques on a test database containing a wide range of explosive detonation experiments (Kingery and Bulmash 1984). The negative phase of the blast wave pressure is not considered in the CONWEP approach. The spherical free airburst option of CONWEP loading was used in this study to generate blast loads on the surfaces of RC slabs facing the point of detonation. The angle of incidence of the blast wave on the exposed surface was taken into account. Only the primary blast wave hitting the slab was considered; blast wave reflections from adjacent surfaces were ignored (Randers-Pehrson and Bannister 1997).

Material Models

The Winfrith material model of the *LS-Dyna* solver was used in this study to model the nonlinear behavior of the concrete (Hallquist 2006). The triaxial state of stress of the Winfrith concrete material is bound by the failure surface proposed by Ottosen (1977, 1979). Hexahedral finite elements were used for the volumetric meshing of the concrete members (Broadhouse and Neilson 1987; Broadhouse 1992; Broadhouse and Attwood 1993; Broadhouse 1995).

A smeared crack formed within the hexahedral element when maximum principal stress exceeded concrete tensile strength in the Winfrith hexahedral elements (Broadhouse and Attwood 1993). When the crack formed, the crack normal stress decayed following a predefined softening curve (Broadhouse 1995). The strain rate effects for the concrete material were not modeled. Disintegration and spalling of the concrete material were taken into account by employing user-defined element erosion criteria based on a combination of the maximum principal strain and negative pressure (Luccioni et al. 2013).

The material model 03 (plastic kinematic type) of the *LS-Dyna* solver was used to simulate the steel material behavior (Hallquist 2006). The reinforcement bars were discretized with two node line elements. The stress-strain curve was idealized as a bilinear relationship. The postyield cyclic response was based on a combination of isotropic and kinematic hardening rules. Rupturing of the steel material was modeled by defining a limiting value of the axial strain. When the rupture strain (ε_r) was reached, the line element was considered to have eroded. Strain rate effects were included using the Cowper-Symonds model (Hallquist 2006; Cowper and Symonds 1957) as follows:

$$\sigma_{yd} = \sigma_y \left(1 + \frac{\epsilon'}{C}\right)^{1/P} \tag{1}$$

where σ_{yd} = dynamic yield stress; σ_y = static yield stress; ϵ' = strain rate; and C and P = parameters of the Cowper-Symonds model (Cowper and Symonds 1957).

In this study, the hexahedral finite elements of the concrete material shared nodes with the line elements of the reinforcing bars. Therefore, a full bond was assumed between the concrete and the reinforcement.

Validation of the Numerical Model

There are a limited number of experimental studies on the blast response of two-way RC slabs in the open literature that provide sufficient data with regard to details on test setup, scaled distance, and experimental results (Rouquand et al. 2003, 2007; Ha et al. 2011). Experiment 2 by Rouquand (Rouquand et al. 2003) was chosen to validate the numerical tool used in this study. Fig. 1 shows the setup of the experiment. A square slab was clamped along the edges with steel frames at the top and bottom. Edge rotations and out-of-plane displacements around the perimeter were fixed, whereas in-plane displacements were permitted. The span length and slab thickness were 1,500 and 100 mm, respectively. The concrete volume was modeled with hexahedral elements having uniform dimensions of 20 × 20 mm on the plan of the slab face and 15 mm through the thickness. The slab had two layers of grid reinforcement with a spacing of 100 mm in each direction and a rebar diameter of 10 mm. This resulted in a total reinforcement ratio of 1.0%. The clear covers at the top and bottom of the cross section were 15 mm thick.

The yield strength of the reinforcement and the compressive and tensile strengths of the concrete were 500, 43, and 3.2 MPa,

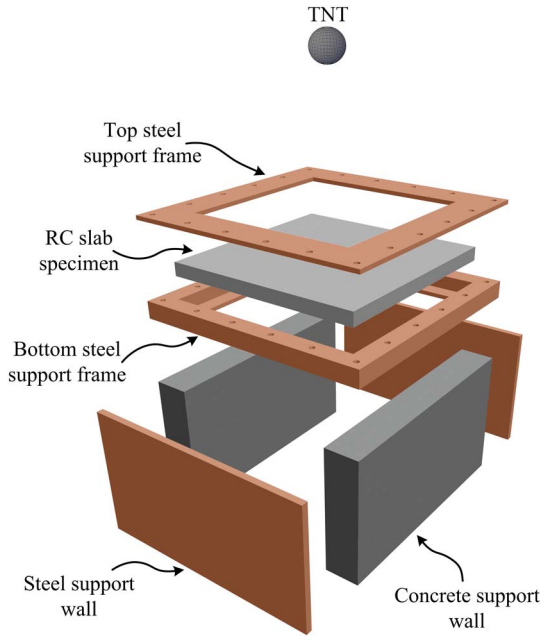

Fig. 1. Test setup of the experiment by Rouquand et al. (2003)

respectively. The charge weight was 40 kg TNT with a standoff distance of 3.6 m to achieve a scaled distance of 1.05 m/kg$^{0.33}$.

Fig. 2 compares pressure and displacement histories at the center of the slab face that was exposed to the detonation. For the experimental measurements and numerical study, the arrival times of the blast wave were 1.89 and 2.00 ms, respectively, and the peak reflected overpressures were 6.4 and 4.3 MPa, respectively.

The experimental study showed that the maximum and permanent mid-deflections of the slab were 29 and 11 mm, respectively, as presented in Fig. 2 (Rouquand et al. 2003). The *LS-Dyna* numerical simulation yielded maximum and permanent mid-deflections of 26 and 9 mm, respectively.

Fig. 3 illustrates the experimentally observed damage pattern and crack formation of the *LS-Dyna* Winfrith concrete material model on the front face of the slab exposed to the detonation. Both the experimental observations and the numerical simulation showed 45° crack line formations around the corners. Fig. 4 compares the experimentally observed damage pattern on the back face of the slab with the damage pattern obtained from the Winfrith concrete model. The crack lines in the middle of the slab formed in a square grid shape, following the arrangement of the rebars placed in both directions of the two-way slab. Both the experimental observations and the numerical simulation showed the formation of

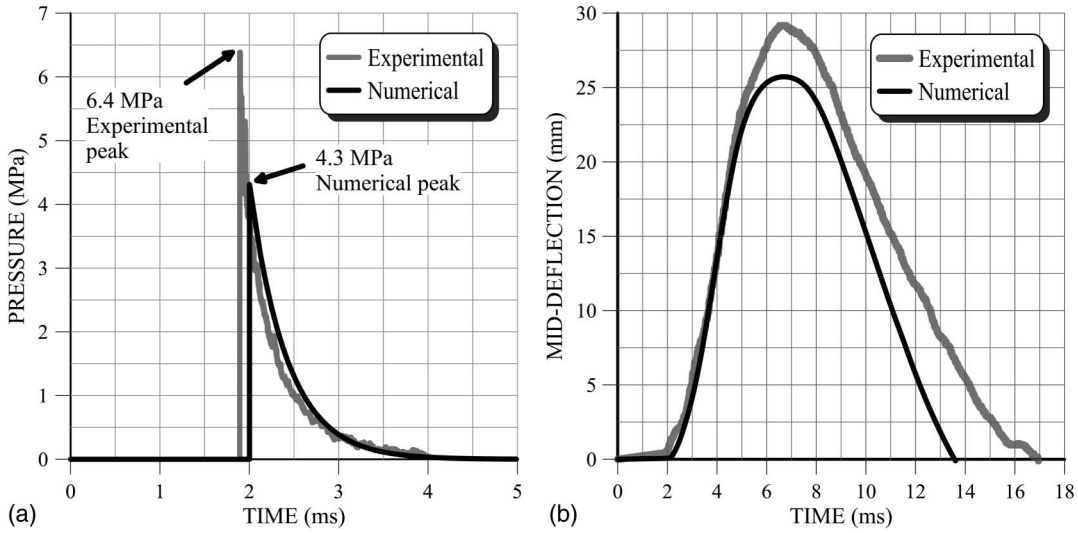

Fig. 2. Pressure time and displacement time histories for the calibration study

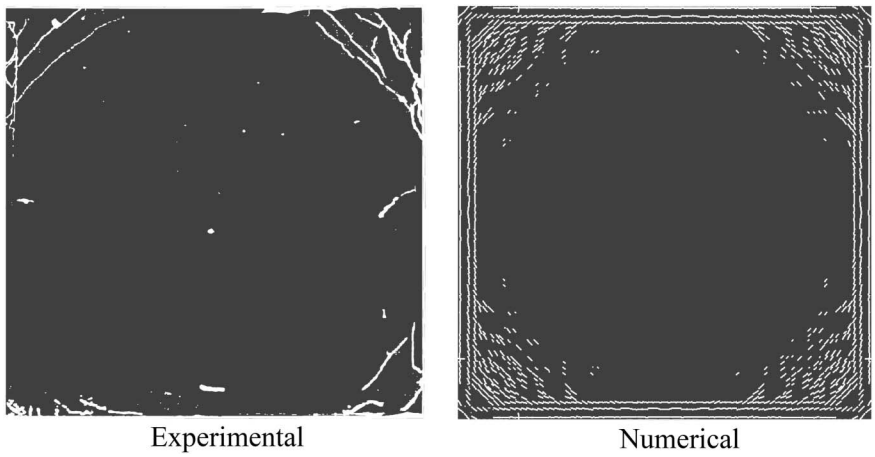

Fig. 3. Crack formation at the top face of the slab directly exposed to the blast pressure

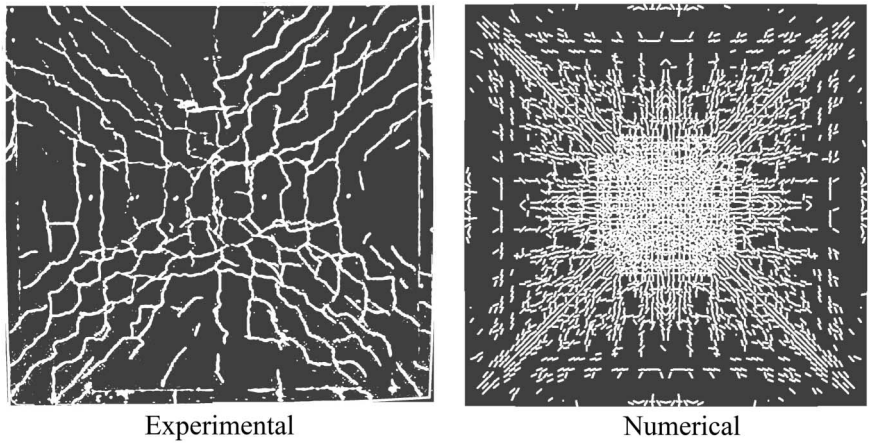

Fig. 4. Crack formation at the bottom face of the slab

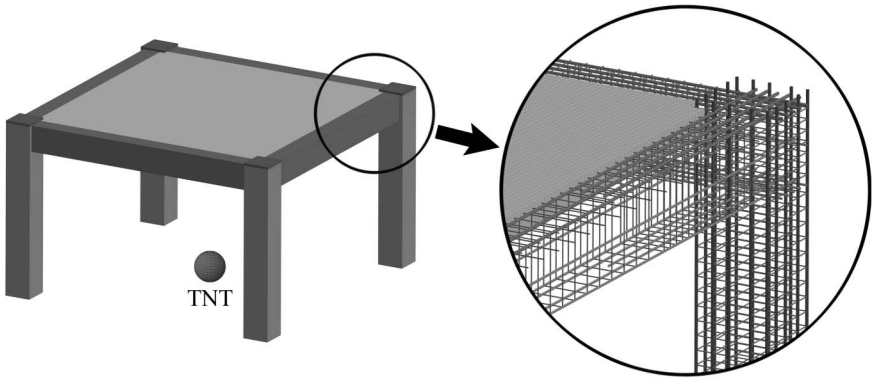

Fig. 5. 3D view of the finite-element model used in the parametric study

diagonal crack lines toward the corners. Overall, the crack formation in the Winfrith material model represented the experimental observations with reasonable accuracy.

Conventional and Protective Design Approaches

In order to compare the airblast responses of two-way RC slabs, two numerical models were constructed. The first slab model (i.e., ACI slab) was designed in accordance with ACI318-14. The second model (i.e., UFC slab) was detailed as per the UFC-3-340-02 for the design of protective structures. The only difference between the two designs was the detailing of the slabs in terms of reinforcement spacing and continuity. In both models, the slabs were supported by a single-story RC frame structure consisting of four beams and four columns. The frame structure provided flexible support to the RC slabs. The beams and columns were designed according to ACI318-14. The longitudinal and transverse reinforcements of the beams and columns were explicitly modeled with the line elements.

Fig. 5 is a three-dimensional (3D) view of the frame structure. The bottom face of the slab was at an elevation of 3 m from the ground. The reinforcement and concrete volume of the structural elements were modeled with two-node line elements and eight-node hexahedral elements, respectively. The finite-element model contained approximately 2.1 million hexahedral elements to represent the concrete volume of the beams, columns, and slabs. The ACI and UFC slabs used 125,000 and 143,000 line elements, respectively. In Fig. 5, the hexahedral elements are transparent in order to show close up the reinforcement details of the beams and columns. The transverse reinforcement consisted of ϕ 8-mm rebars and was placed at 80- and 160-mm intervals for the confinement and central zones, respectively, of the frame elements. Fig. 6 shows the cross-sectional dimensions and reinforcement details of the beams and columns of the frame. The clear cover was 30 mm thick for the frame members and slab.

For the conventional slab design according to ACI 318, only the dead and live loads due to gravity were considered. A design live load of 5 kN/m^2 was assumed, which represented the nominal load for parking garage slabs. The design load factors used for the dead and live loads were 1.2 and 1.6, respectively.

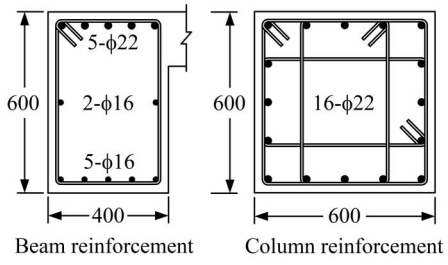

Fig. 6. Longitudinal reinforcement details and cross-sectional dimensions of the beams and columns (all dimensions and rebar diameters in millimeters)

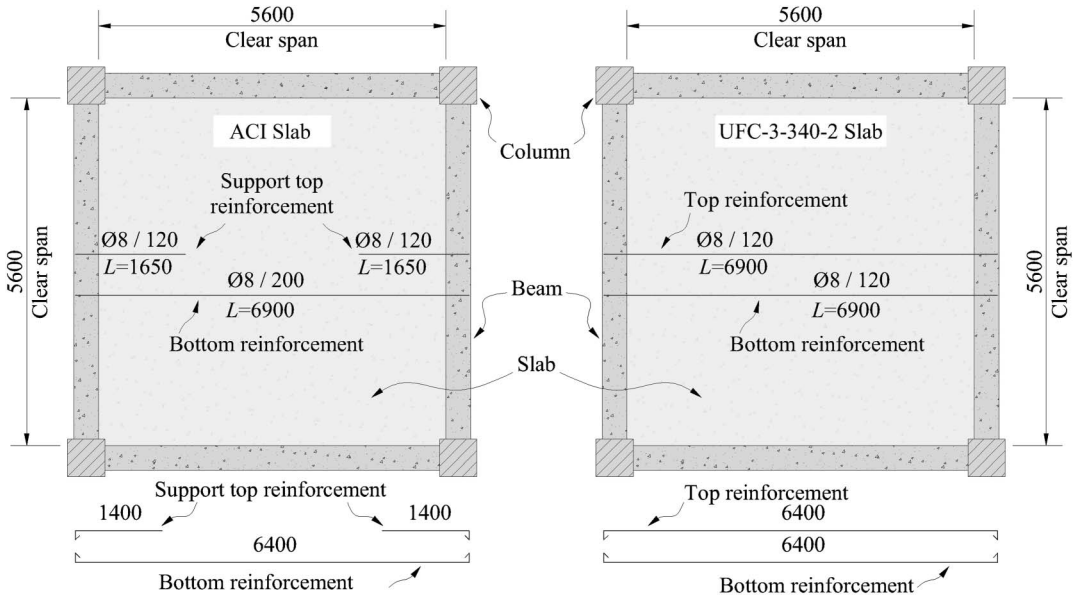

Fig. 7. Reinforcement details of the ACI and UFC slabs (all dimensions in millimeters)

The assumed explosive charge weight for the UFC slab was 8-kg TNT detonating at a standoff distance of 2 m below the bottom face of the slab. The slab was designed for a 2° support rotation. The scaled distance Z for the explosion was 1.00 m/kg$^{0.33}$. This scaled distance is defined as a close-in range explosion in UFC-3-340-02 (DoD 2008). Therefore, an impulse-based design was carried out. The reflected impulse per unit area used in the design calculation was approximately 1,130 Pa · s.

The dimensions and reinforcement detailing of the ACI and UFC slabs are shown in Fig. 7. The clear span length L was 5,600 mm. The reinforcement of the square-shaped slab was symmetric in the two orthogonal directions on its plane. For the purpose of clarity, Fig. 7 only shows the reinforcement in one direction.

The ACI slab had continuous bottom reinforcement of ϕ 8-mm rebars with 200-mm spacing. Its top reinforcement consisted of ϕ 8-mm rebars with 120-mm spacing and extended to a distance of one-quarter of the span length from the supports in both directions. The top reinforcement was discontinuous, and the slab midspan had only bottom reinforcement. There were 28 and 46 top and bottom rebars, respectively, in each direction for a total reinforcement ratio of 0.37%. Figs. 8(a and b) show the ACI slab's top and bottom reinforcement configurations, respectively.

The UFC slab had continuous and symmetric top and bottom reinforcement layers consisting of ϕ 8-mm rebars with 120-mm spacing, as illustrated in Fig. 8(c). There were 46 rebars at the top and bottom of the cross section to yield a total reinforcement ratio of 0.46%.

The material properties for both slabs were assumed to be the same. The unconfined compressive strength and tangent elastic modulus of the concrete were set to 30 and 28 GPa, respectively. The concrete hexahedral elements eroded when the maximum principal strain exceeded 0.05. The selected erosion criterion for the concrete material was within the range of values reported in the literature review by Luccioni (Luccioni et al. 2013). The steel reinforcement yield strength and elastic modulus were set to 420 and 200 GPa, respectively. The slab thickness was 180 mm. The concrete covers at the top and bottom of the slab cross section were each 30 mm thick. The strain rate effects on the rebars were included

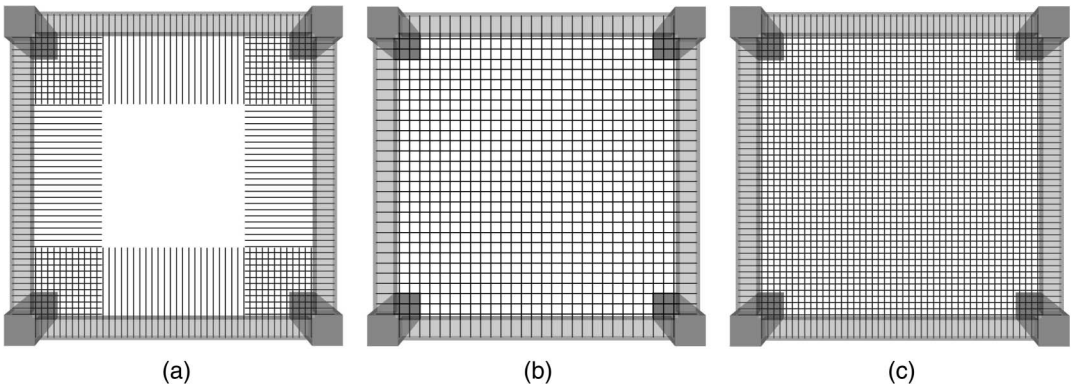

Fig. 8. Modeling of slab reinforcement with two-node line elements in the numerical study: (a) discontinuous top reinforcement of the ACI slab with 120 mm spacing; (b) continuous bottom reinforcement of the ACI slab with 200 mm spacing; (c) top and bottom reinforcements of the UFC slab with 120 mm spacing

J. Perform. Constr. Facil., 2017, 31(3): 04016105

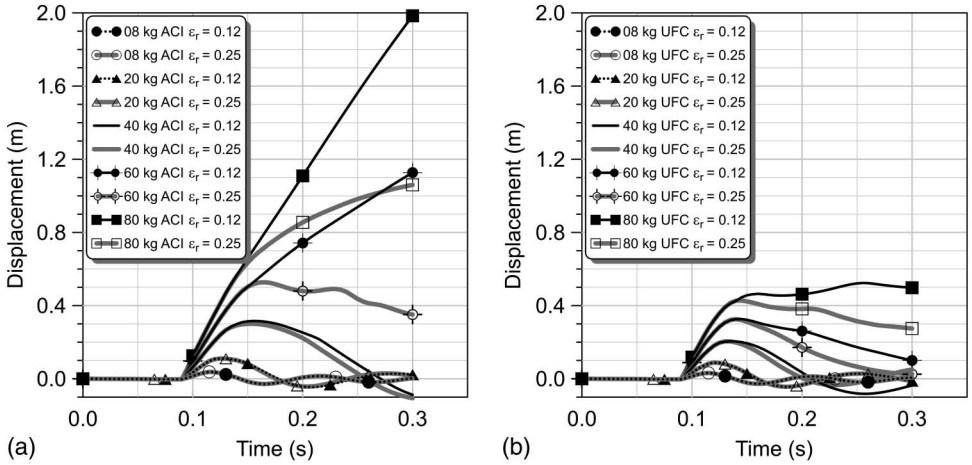

Fig. 9. Displacement-time history plots of the ACI and UFC slabs: (a) ACI slab; (b) UFC slab

using values of 424 and 4.73 for the nondimensional constants of C and P, respectively, in the Cowper-Symonds model expressed by Eq. (1) (Malvar and Crawford 1998). The rebar rupture was modeled defining a limiting value for the maximum principal strain.

Parametric Study on the Uplift Response of RC Slabs

A parametric study was conducted on the ACI and UFC slabs for different close-in blast load scenarios. This was achieved by detonating various charge weights under the slabs as shown in Fig. 5. The reflected pressure for the charge weight of 8 kg was 5,006 kPa and increased to 41,900 kPa for the charge weight of 80 kg. The reflected impulses of the charge weights of 8 and 80 kg were 1,118 and 8,406 Pa · s, respectively. The scaled distances of the charge weights of 8 and 80 kg were 1.00 and 0.46 m/kg$^{0.33}$, respectively.

Another parameter investigated in this study was the magnitude of the reinforcement rupture strain. ASTM A615 requires a minimum strain at failure of 0.09 (ASTM 2015). The literature survey related to rebar rupture strain ranged between 0.12 and 0.25 (Malvar 1998; Malvar and Crawford 1998; Mo and Kuo 1995; Ammann et al. 1982; Wang et al. 1978). Therefore, the envelope limits of 0.12 and 0.25 were used in this study for the rupture strains of the reinforcements. The effects of charge weight and rupture strain on the uplift response of the slabs were determined.

Results of the Parametric Study

This section presents the midspan displacement histories, support rotations, damage patterns, and failure modes of the parametric study for the *LS-Dyna* simulations of the ACI and UFC slabs. In order to categorize the damage, the main failure modes and distinctive crack patterns were considered. The effect of rebar rupture strain on slab performance was examined.

Figs. 9(a and b) show the midspan displacement histories of the ACI and UFC slabs, respectively. Table 1 gives the number of ruptured support rebars along with maximum midspan displacements (δ_{mid}) and corresponding support rotations (θ_{sup}). The midspan displacements δ_{mid} were obtained from the nodal displacements of the *LS-Dyna* simulation. The support rotation θ_{sup} was calculated using the clear span length L in Eq. (2):

$$\theta_{sup} = \tan^{-1}\left(\frac{\delta_{mid}}{\frac{L}{2}}\right) \quad (2)$$

The midspan displacements for the 80-kg ACI slab exhibited a continuously increasing trend with rebar rupture strains (ε_r) of 0.12 and 0.25. The displacement showed the same trend for the 60-kg ACI with a rebar rupture strain of 0.12. In these simulations, a significant portion of the support rebars ruptured, which led to the complete failure of the slabs. The midspan of the slab moved upward in a kinematic motion; a rebound behavior of the slab was not observed. The support rotations were in excess of 20°. Therefore, the corresponding midspan displacements and support rotations for these simulations are designated "N/A" (not available) for these simulations in Table 1.

The damage progression of the ACI and UFC slabs started with cracking of the concrete at the bottom support sections, was

Table 1. Charge Weights, Number of Ruptured Rebars on a Single Slab Edge, Midspan Displacement (δ_{mid}), and Support Rotation (θ_{sup})

W_{TNT} (kg)	Design code	Rebar rupture strain, ε_r	Number of upper support rebars ruptured	Number of lower support rebars ruptured	δ_{mid} (m)	θ_{sup} (degrees)
8	ACI	0.12	0/46	0/28	0.038	0.8
20	ACI	0.12	0/46	14/28	0.111	2.3
40	ACI	0.12	22/46	22/28	0.316	6.4
60	ACI	0.12	34/46	24/28	N/A	N/A
80	ACI	0.12	42/46	24/28	N/A	N/A
8	ACI	0.25	0/46	0/28	0.038	0.8
20	ACI	0.25	0/46	0/28	0.111	2.3
40	ACI	0.25	0/46	18/28	0.301	6.1
60	ACI	0.25	26/46	20/28	0.528	10.7
80	ACI	0.25	34/46	22/28	N/A	N/A
8	UFC	0.12	0/46	0/46	0.032	0.7
20	UFC	0.12	0/46	0/46	0.088	1.8
40	UFC	0.12	6/46	34/46	0.205	4.2
60	UFC	0.12	32/46	38/46	0.327	6.7
80	UFC	0.12	46/46	42/46	0.524	10.6
8	UFC	0.25	0/46	0/46	0.032	0.7
20	UFC	0.25	0/46	0/46	0.089	1.8
40	UFC	0.25	0/46	0/46	0.205	4.2
60	UFC	0.25	0/46	26/46	0.326	6.6
80	UFC	0.25	32/46	34/46	0.428	8.7

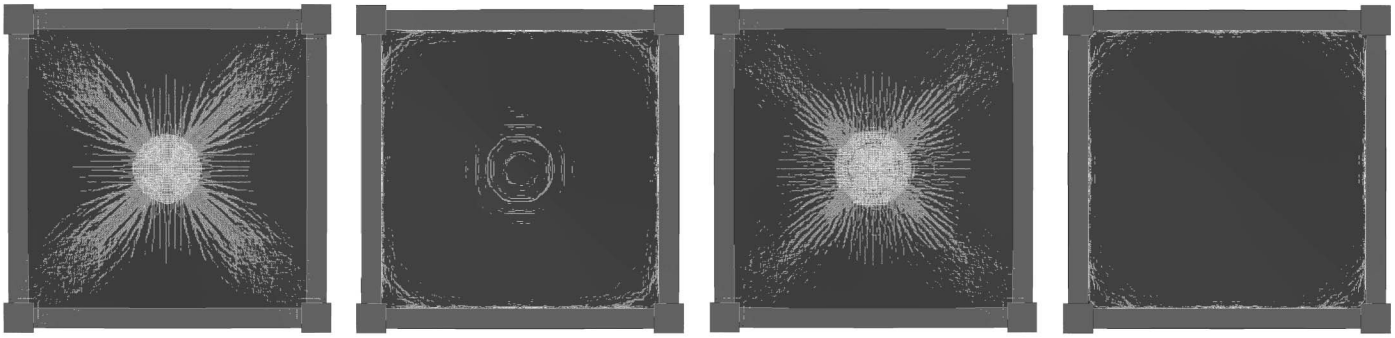

Fig. 10. Top and bottom crack patterns in the ACI and UFC slabs for the 40-kg charge weight with a rupture strain of $\varepsilon_r = 0.12$: (a) top face crack formation, ACI slab; (b) bottom face crack formation, ACI slab; (c) top face crack formation, UFC slab; (d) bottom face crack formation, UFC slab

Fig. 11. Damage states and crack patterns in the ACI and UFC slabs for the 80-kg charge weight: (a) ACI slab, $\varepsilon_r = 0.12$; (b) ACI slab, $\varepsilon_r = 0.25$; (c) UFC slab, $\varepsilon_r = 0.12$; (d) UFC slab, $\varepsilon_r = 0.25$

followed by damage accumulation at the midspan, and finally ended with the yielding or rupturing of the upper support rebars.

Fig. 10(a) illustrates the localized diagonal crack pattern for the ACI slab with a rupture strain of 0.12 and subjected to a charge weight of 40 kg. The crack formation resembled the typical yield line pattern for two-way slabs, and was observed in the simulation results of the ACI slab for all charge weight detonations. Fig. 10(b) shows the cracks near the support region at the bottom of the ACI slab.

Additional damage at the midspan of the ACI slab was also observed for charge weights of 60 and 80 kg, both of which punched out a square segment in the midspan of the slabs, where no upper reinforcement was provided by the gravity design. This failure mode is illustrated in Figs. 11(a and b) for the charge weight of 80 kg and rupture strains of 0.12 and 0.25, respectively.

The typical yield line pattern presented earlier for the ACI slab was not apparent in the simulation results for the UFC slab. In general, the UFC slab acted as a whole and the damage was distributed throughout the slab span.

The UFC slabs performed better than the ACI slabs in terms of deformation capacity and damage state. The rebar rupture strain of 0.25 improved the deformation capacities of both slabs. For the charge weight of 60 kg, the rupture strain by itself governed the failure. The UFC slab with a rebar rupture strain of 0.25 survived the blast, whereas the UFC slab with a rupture strain of 0.12 failed when subjected to the 60-kg charge weight.

Discussion

By using 3D solid elements to model the beams and columns supporting the slabs, a more accurate representation of support conditions was obtained in this study. The joint ACI-ASCE Committee 421 (ACI-ASCE-421 2015) suggests using 3D solid elements or one-dimensional (1D) line elements rather than a simplified pin or fixed support conditions at the slab boundaries. Considering the physical size of the connected structural members, the finite length of the joint was also explicitly taken into account, as illustrated by the close-up view of the finite-element model in Fig. 5.

Table 3–2 of ASCE 59-11 (ASCE 2011) provides the following limits for the support rotation (θ_{sup}) of double-reinforced slabs without shear reinforcement: 2° for moderate damage, 5° for heavy damage, and 10° for hazardous damage. Park and Gamble (2000) considered a safe maximum value for the midspan displacement to be 10% of the clear span length L based on experiments conducted by Keenan (1969) and Black (1975). In fact, Black reported that the reinforcing bars ruptured at a midspan displacement of 0.15 L. The corresponding support rotations for the 0.10- and 0.15-L midspan displacements were 11° and 17°, respectively.

Fig. 11 shows the damage states of the slabs for the 80-kg ACI simulations. The blast punched out the middle portion of the slab, which led to hazardous mode failure as illustrated in Figs. 11(a and b). A similar observation can be made for the case of the 80-kg UFC slab with a rupture strain of 0.12. Fig. 11(c) illustrates the failure of the slab's support rebars. Table 1 gives the support rotation as 10.6°. Based on the results of the parametric study, the failure of the investigated slabs occurred at a support rotation of approximately 11°.

The numerically obtained maximum support rotations of the slabs were in agreement with the experimentally observed results by Keenan (1969). The only exception was the ACI slab with a rupture strain of 0.12, which could not go beyond a maximum support rotation of 6.4° for the range of charge weights

considered. The number of ruptured rebars reported in Table 1 indicated loss of tensile membrane capacity for the ACI slab with a rupture strain of 0.12 subjected to a charge weight of 60 kg. The premature failure of the ACI slab was due to the combined effects of discontinuous upper reinforcements and a low rebar rupture strain value.

The displacement time histories of the failed slabs shown in Fig. 9(a) included not only the slab deformations but also the rigid body motion of the disintegrated parts on which the displacements were traced. The disintegrated middle parts of the ACI slabs with rupture strains of 0.12 and 0.25 are illustrated in Figs. 11(a and b). The larger displacement of the ACI slab with a rupture strain of 0.12 did not indicate a larger ductility capacity compared with the ACI slab with a rupture strain of 0.25 when subjected to a charge weight of 80 kg.

In order to demonstrate the effectiveness of rebar rupture strain, the performance of the UFC slab with a 0.12 rupture strain was compared with that of a UFC slab with a 0.25 rupture strain under a 40-kg charge weight. At the end of the analysis, both slabs experienced almost the same amount of midspan displacement, which corresponded to a support rotation of 4.2°. Blast design standards quantify damage with respect to support rotations alone. In the current study, however, all of the support rotations were the same whereas the numbers of ruptured rebars were different. The UFC slab with a rupture strain of 0.12 had 34 rebars ruptured, whereas the UFC slab with a rupture strain of 0.25 had no rebars ruptured. This implies that the rebar rupture strain should be considered for quantifying the damage in detail.

Because of uplift deformation, the bottom support rebars were subjected to larger strains; this caused them to rupture before the upper support rebars.

Conclusions

Blast performance analyses of the ACI gravity and UFC protective designs for RC slabs revealed that ultimate capacity was governed by tensile membrane action and that the most critical sections were the slab supports. The failure mode was initiated by the bottom support rebars rupturing first, followed by the midspan rebars and then the upper support rebars.

The UFC slabs performed better than the ACI slabs. Even though only factored gravity loads were considered in the design approach, the numerical simulations showed that the ACI slabs resisted charge weights of 8 and 20 kg for rebar rupture strains of 0.12 and 0.25, respectively, without significant damage. The numerical results of this study quantified the ACI slabs' limited capacities for tensile membrane action. The UFC slabs withstood charge weights of 20 and 40 kg for rebar rupture strains of 0.12 and 0.25, respectively, without any rebar rupture.

According to the results of the parametric simulation study for a rebar rupture strain of 0.12, the ACI and UFC slab designs sustained support rotations of 0.8° and 1.8° without any rebar rupture. Increasing the rebar rupture stain to 0.25 increased the support rotation capacities to 2.3° and 4.2° for the ACI and UFC slab designs, respectively. The higher rebar rupture strain of 0.25 significantly improved the deformation capacity of the slabs compared with the lower value of 0.12. Slabs with discontinuous reinforcement and low rebar rupture strains may fail prematurely under blast loads and possess limited support rotation capacities.

Protective design codes define slab damage based on measured support rotations. However, the results of this study showed that support rotation by itself is not sufficient to determine or define damage. Based on the findings of this study, it is recommended that the effect of rebar rupture strain on design damage level categories also be included.

Bond failure between concrete and steel reinforcements may affect slab behavior under blast loads. Therefore, it is recommended that bond-slip models be considered in future numerical studies. Further experimental data are needed to support the conclusions of this study and to validate the presented numerical results.

Acknowledgments

The author is grateful for the funding provided by the Turkish Scientific and Technological Research Council (TUBITAK) through Grant 107M002 and for that provided by the Bogazici University Research Fund through Contract 07HT102.

References

ACI (American Concrete Institute). (2014). "Building code requirements for structural concrete and commentary." *ACI 318-14*, Farmington Hills, MI.

ACI-ASCE-421. (2015). "Guide to design of reinforced two-way slab systems." *ACI-ASCE 421.3R-15*, Farmington Hills, MI.

Ammann, W., Mühlematter, M., and Bachmann, H. (1982). "Stress–strain behaviour of non-prestressed and prestressed reinforcing steel at high strain rates." *Proc., Interassociation Symp. on Concrete Structures under Impact and Impulsive Loading*, BAM (Bundesanstalt fuer Materialpruefung), Berlin.

ASCE. (2011). "Blast protection of buildings." Reston, VA.

ASTM. (2015). "Standard specification for deformed and plain carbon-steel bars for concrete reinforcement." West Conshohocken, PA.

Black, M. S. (1975). "Ultimate strength study of two-way concrete slabs." *J. Struct. Div.*, 101(1), 311–324.

Broadhouse, B. J. (1992). "DYNA3D analysis of cone crack formation due to heavy dropped loads on reinforced concrete floors." *Proc., Structures under Shock and Impact Conf.*, WIT Press, Dorset, U.K.

Broadhouse, B. J. (1995). "The Winfrith concrete model in LS-DYNA3D." *Rep. No. SPD/D(95)363*, Atomic Energy Authority, Winfrith Technology Centre, Dorset, U.K.

Broadhouse, B. J., and Attwood, G. J. (1993). "Finite element analysis of the impact response of reinforced concrete structures using DYNA3D." *Proc., XII Structural Mechanics in Reactor Technology Conf.*, Stuttgart, Germany, International Association for Structural Mechanics in Reactor Technology, Dorset, U.K.

Broadhouse, B. J., and Neilson, A. J. (1987). "Modelling reinforced concrete structures in DYNA3D." *Proc., DYNA3D User Group Conf.*, London.

Cowper, G., and Symonds, P. S. (1957). "Strain hardening and strain rate effects in the impact loading of cantilever beams." *Rep. No. 28*, Brown Univ., Providence, RI.

DoD (Department of Defense). (2008). "Unified facilities criteria: Structures to resist the effects of accidental explosions." Washington, DC.

FEMA (Federal Emergency Management Agency). (1996). "The Oklahoma City bombing: Improving building performance through multi-hazard mitigation." *Rep. No. 277*, Washington DC.

FEMA (Federal Emergency Management Agency). (2005). "Blast-resistance benefits of seismic design. Phase 1 study: Performance analysis of reinforced concrete strengthening systems applied to the Murrah Federal Building design." *Rep. No. 439A*, Washington, DC.

FEMA (Federal Emergency Management Agency). (2008). "Incremental protection for existing commercial buildings from terrorist attack." *Rep. No. 459*, Washington, DC.

Garcia, L., Pujol, S., Ramirez, J., and Sozen, M. (2006). "Structural effects of the February 7, 2003, bombing of the El Nogal Building in Bogotá, Colombia." Purdue Univ. School of Civil Engineering, West Lafayette, IN.

Ha, J., Yi, N., Choi, J., and Kim, J. J. (2011). "Experimental study on hybrid CFRP-PU strengthening effect on RC panels under blast loading." *Compos. Struct.*, 93(8), 2070–2082.

Hallquist, J. (2006). "LS–Dyna theory manual." Livermore Software Technology Corporation, Livermore, CA.

Hyde, D. (1993). "User's guide for microcomputer programs CONWEP and FUNPRO: Applications of TM 5-855-1, 'Fundamentals of protective design for conventional weapons.'" *Rep. No. SL-88-1*, U.S. Army Corps of Engineers, Waterways Experiment Station, Vicksburg, MS.

Keenan, W. A. (1969). "Strength and behavior of restrained reinforced concrete slabs under static and dynamic loadings." *Rep. No. R621*, U.S. Naval Civil Engineering Laboratory, Port Hueneme, CA.

Kingery, C., and Bulmash, G. (1984). "Air-blast parameters from TNT spherical air burst and hemispherical surface burst." *Rep. No. ARBRL-TR-02555*, Ballistic Research Laboratory, Aberdeen Proving Ground, Aberdeen, MD.

Krauthammer, T. (2008). *Modern protective structures*, CRC Press, Boca Raton, FL.

Lawver, D., Daddazio, R., Oh, G., Lee, C., Pifko, A., and Stanley, M. (2003). "Simulating the response of composite reinforced floor slabs subjected to blast loading." *Proc., IMECE'03 Congress*, ASME, Washington, DC, 1–7.

Longinow, A., and Mniszewski, K. R. (1996). "Protecting buildings against vehicle bomb attacks." *Pract. Period. Struct. Des. Constr.*, 10.1061/(ASCE)1084-0680(1996)1:1(51), 51–54.

LSTC (Livermore Software Technology Corporation). (2015). "LS-Dyna: Keyword user's manual." Livermore, CA.

Luccioni, B. M., Aráoz, G. F., and Labanda, N. A. (2013). "Defining erosion limit for concrete." *Int. J. Protective Struct.*, 4(3), 315–340.

Malvar, L. J. (1998). "Review of static and dynamic properties of steel reinforcing bars." *ACI Mater. J.*, 95(5), 609–614.

Malvar, L. J., and Crawford, J. E. (1998). "Dynamic increase factors for steel reinforcing bars." *Proc., DDESB, 28th Dept. of Defense Explosives Safety Seminar*, Engineers' Society of Western Pennsylvania, Orlando, FL.

Mo, Y. L., and Kuo, J. Y. (1995). "Effect of welding on ductility of rebars." *J. Mater. Civ. Eng.*, 7(4), 283–285.

Ottosen, N. (1977). "A failure criterion for concrete." *J. Eng. Mech. Div.*, 103(4), 527–535.

Ottosen, N. (1979). "Constitutive model for short-time loading of concrete." *J. Eng. Mech. Div.*, 105(1), 127–141.

Park, R., and Gamble, W. L. (2000). *Reinforced concrete slabs*, Wiley, New York.

Randers-Pehrson, G., and Bannister, K. (1997). "Airblast loading model for DYNA2D and DYNA3D." *Rep. No. ARL-TR-1310*, U.S. Army Research Laboratory, Aberdeen, MD.

Razaqpur, A. G., Tolba, A., and Contestabile, E. (2007). "Blast loading response of reinforced concrete panels reinforced with externally bonded GFRP laminates." *Compos. Part B*, 38(5–6), 535–546.

Rouquand, A., Laurensou, R., and Cremoux, J. L. (2003). "Behavior of concrete panels to HE charges and evaluation of the simplified method MAXDALLE." *Proc., ISIEMS-2003, Int. Conf. on Interaction of the Effects of Munitions with Structures*, German Federal Ministry of Defense, Bèdes, France.

Wang, P. T., Shah, S., and Naaman, A. E. (1978). "High-strength concrete in ultimate strength design." *J. Struct. Div.*, 104(11), 1761–1773.